Dynamics Study of the OH + O_3 Atmospheric Reaction with Both Reactants Vibrationally Excited

Lei Zhang,[†] Pingya Luo,[‡] Zhiyu Huang,[†] and António J. C. Varandas*[,#]

School of Chemistry and Chemical Engineering, Southwest Petroleum University, Chengdu 610500, Sichuan, P. R. China, State Key Laboratory of Oil & Gas Reservoir Geology and Exploitation, Southwest Petroleum University, Chengdu 610500, Sichuan, P. R. China, and Departamento de Química, Universidade de Coimbra, 3004-535 Coimbra, Portugal

Received: September 25, 2006; In Final Form: November 6, 2006

The dynamics of the title five-atom atmospheric reaction is studied by the quasiclassical trajectory method for vibrational states of OH over the range $2 \leq v \leq 9$ and initial vibrational energies of O_3 between 9 and 21 kcal mol^{-1} using a previously reported double many-body expansion potential energy surface for HO_4-(^2A). The results show that the reaction is controlled by both capture- and barrier-type mechanisms, with the rate constants depending strongly on the reactants' internal energy content. Also suggested from the magnitude of the calculated rate coefficients is that the title processes may not be ignorable when studying the stratospheric ozone budget.

1. Introduction

Collisional processes involving vibrationally excited molecules have a long and rich history in the development of reaction dynamics as they offer a firm basis for the modern study of the chemistry and physics of such species. Uncovering their dynamics also greatly enhances our understanding of areas with practical interest, namely, atmospheric chemistry, combustion, and unimolecular decomposition of activated species.[1−12] Of particular importance is the role of internal energy in the collisional process, especially for energies close to the dissociation threshold. Indeed, the internal-energy dependence holds important information about the behavior of the colliding species, providing clues for the microscopic details of the intermolecular energy transfer.[13]

Vibrationally excited hydroxyl radicals [hereafter denoted by OH(v)] are generated in the upper stratosphere and mesosphere by the reaction of hydrogen atoms with ozone, and at lower altitudes (ref 14, and references therein) through the reaction of oxygen atoms in the lowest electronic singlet state with water molecules, O(^1D) + H_2O. Being chain carriers in a number of systems and playing a prominent role in the study of the infrared emission from the earth's upper atmosphere, they have not surprisingly received considerable experimental and theoretical attention over the years. Indeed, spectral and temporal information from such emissions is commonly used in monitoring atmospheric phenomena and in creating models of atmospheric chemistry and kinetics (see, for example, refs 10, 12, and 15 and references therein).

Because of its atmospheric importance, the set of collisional processes involving OH(v) became one of the most extensively studied examples of collisional dynamics involving highly vibrationally excited species. In fact, the past decade has seen considerable effort, both experimental and theoretical, aimed at yielding a complete picture for OH(v) colliding with a variety of atmospheric partners such as O_2, O_3, N_2, CO_2, NH_3, etc. Although significant progress has been made in measuring the vibrational level dependence of the total removal rate constants in these collisional processes,[15−28] an important natural species of the atmosphere that is essentially absent from such a progress list is vibrationally excited O_3 [this is hereafter denoted through its vibrational energy content as $O_3(E_v)$]. This provided a strong motivation for carrying out the present study of the OH(v) + $O_3(E_v)$ reaction.

Of course, a potential energy surface (or eventually more) is required for studying the title collisional processes, which became available in 2000 with our publication[29] of a global function using double many-body expansion theory (ref 31 and references therein). Such theoretical work has been followed by one of us[9] through limited electronic structure calculations carried out using a complete-active-space self-consistent-field wave function (which comprised nine active electrons and nine active molecular orbitals) and subsequently by other authors[32,33] using the same as well as other levels of ab initio theory. In particular, Mansergas and Anglada[33] performed extensive calculations at various levels of ab initio theory aimed at the study of the OH···O_3 van der Waals complex in the reactants channel.[33] They have predicted two minima (of $^2A'$ and $^2A''$ symmetries) with well depths of 0.87 and 0.67 kcal mol^{-1} (respectively), which compare with the value of 1.5 kcal mol^{-1} predicted by the double many-body expansion (DMBE) potential energy surface[29] and the experimental prediction of Engdahl and Nelander[34] that such a minimum should be weaker than 1.2 kcal mol^{-1}.

In a series of papers,[35,36] we provided detailed information on collisions of vibrationally excited hydroxyl radicals with ozone in its ground vibrational state by using the above HO_4 DMBE potential energy surface. Good agreement was obtained with the available experimental data. However, our understanding of the collisional processes of these species is far from

* To whom correspondence should be addressed. E-mail: varandas@qtvs1.qui.uc.pt.
[†] School of Chemistry and Chemical Engineering, Southwest Petroleum University.
[‡] State Key Laboratory of Oil & Gas Reservoir Geology and Exploitation, Southwest Petroleum University.
[#] Departamento de Química, Universidade de Coimbra.

10.1021/jp066273j CCC: $33.50
Published on Web 12/21/2006

TABLE 1: Summary of the OH(v) + O_3(E_v) Trajectory Calculations

(v, E_v)	E_{tr} kcal mol^{-1}	b_{max} a_0	HO_2^*/HO_2 + OH N_r	$O_2 + O_2 + H$ N_r	O_2 + OH + O N_r	$\sigma^{total} \pm \Delta\sigma^{total}$ a_0^2
(2, 9)	1.0	9.64	109	31	2	20.72 ± 1.68
	2.0	8.13	102	24	1	13.17 ± 1.13
	4.0	7.18	99	33	1	10.77 ± 0.90
	6.0	7.18	116	36	3	12.56 ± 0.97
	8.0	7.18	141	44	12	15.96 ± 1.08
	12.0	7.56	180	56	17	22.71 ± 1.33
(4, 9)	1.0	9.83	153	136	38	49.60 ± 2.51
	2.0	9.45	116	79	33	31.97 ± 1.99
	4.0	8.50	102	86	27	24.42 ± 1.57
	6.0	7.94	121	71	39	22.86 ± 1.41
	8.0	7.75	132	99	47	26.21 ± 1.46
	12.0	7.37	172	156	78	34.64 ± 1.54
(4, 15)	1.0	10.39	162	155	86	68.38 ± 3.04
	2.0	10.20	111	120	60	47.60 ± 2.58
	4.0	9.07	96	100	72	34.64 ± 1.97
	6.0	8.69	105	124	62	34.54 ± 1.87
	8.0	8.13	136	129	81	35.88 ± 1.75
	12.0	7.75	189	160	106	42.90 ± 1.77
(4, 21)	1.0	10.58	159	253	176	103.44 ± 3.58
	2.0	10.39	110	225	161	84.16 ± 3.28
	4.0	10.20	97	180	148	69.52 ± 2.99
	6.0	10.20	96	150	150	64.77 ± 2.92
	8.0	9.45	108	162	173	62.12 ± 2.60
	12.0	9.26	124	181	175	64.65 ± 2.57
(6, 9)	1.0	10.39	104	241	65	69.57 ± 3.06
	2.0	10.02	77	187	62	51.37 ± 2.60
	4.0	9.26	74	141	55	36.36 ± 2.06
	6.0	8.88	70	144	62	34.20 ± 1.91
	8.0	7.94	98	199	88	38.10 ± 1.74
	12.0	7.75	120	266	98	45.64 ± 1.81
(6, 15)	1.0	10.39	107	302	120	89.76 ± 3.35
	2.0	10.20	80	249	92	68.86 ± 2.98
	4.0	9.26	56	195	92	46.20 ± 2.27
	6.0	9.07	70	175	109	45.75 ± 2.21
	8.0	8.69	85	195	120	47.48 ± 2.12
	12.0	8.13	123	258	146	54.66 ± 2.04
(6, 21)	1.0	10.96	88	359	215	124.92 ± 3.97
	2.0	10.77	94	291	177	102.42 ± 3.66
	4.0	10.39	71	238	175	82.13 ± 3.25
	6.0	10.39	66	209	174	76.19 ± 3.17
	8.0	9.83	68	232	185	73.56 ± 2.91
	12.0	9.84	89	218	208	75.14 ± 2.85
(9, 9)	1.0	10.58	60	280	132	83.03 ± 3.34
	2.0	10.20	38	258	123	68.54 ± 2.98
	4.0	9.64	29	207	103	49.46 ± 2.45
	6.0	9.07	40	226	95	46.66 ± 2.22
	8.0	8.13	52	277	136	48.22 ± 1.96
	12.0	7.94	72	333	140	53.93 ± 1.97
(9, 15)	1.0	11.15	26	311	181	101.15 ± 3.83
	2.0	10.39	41	305	193	91.46 ± 3.37
	4.0	9.83	41	268	128	66.28 ± 2.80
	6.0	9.45	51	264	140	63.81 ± 2.63
	8.0	9.07	56	275	157	63.07 ± 2.48
	12.0	8.50	76	339	180	67.59 ± 2.32
(9, 21)	1.0	11.72	88	359	215	142.74 ± 4.54
	2.0	11.34	94	291	177	113.49 ± 4.06
	4.0	10.96	71	238	176	91.52 ± 3.62
	6.0	10.58	66	236	174	83.73 ± 3.35
	8.0	10.20	68	241	185	80.80 ± 3.15
	12.0	9.83	89	239	234	85.24 ± 3.05

complete since the role of reactants internal energy in such processes has practically been left unanswered. Thus, a need exists for obtaining insights into its behavior and to identify the 1 important physical parameters and propensities in such collisional processes. In the present work, we extend previous calculations to higher internal energies by reporting a detailed study of the title multichannel reaction:

$$OH(v) + O_3(E_v) \rightarrow HO_2^*/HO_2 + O_2 \quad (1)$$

$$\rightarrow O_2 + O_2 + H \quad (2)$$

$$\rightarrow O_2 + OH + O \quad (3)$$

where the vibrational quantum number of OH is chosen to vary over the range $2 \leq v \leq 9$, and the total vibrational energy content of O_3 between 9 and 21 kcal mol^{-1}. Such combinations will be denoted by (v, E_v), with E_v assumed to be given in kcal mol^{-1}. Note that the star in reaction 1 indicates that the formed hydroperoxyl molecules have an internal energy above the dissociation limit. Of particular relevance in this study is the clear prediction of a substantial and specific enhancement of reactivity due to vibrational excitation of both reactants. As in previous work, we will employ the well-established quasiclassical trajectory (QCT) method and the $HO_4(^2A)$ DMBE potential energy surface.[29] Although the presence of the light hydrogen

atom suggests that an accurate quantum dynamics approach is required for obtaining accurate results, such an approach is currently far beyond our capabilities (ref 8 and references therein) for systems with more than four atoms. Moreover, the high-energy regimes involved and the quality of previous results[10] (for cases as extreme as $H + H_2$, see ref 30 and references therein) suggest that the QCT approach is here too well justified.

The paper is organized as follows. Section 2 provides a brief survey of the methodology, while the dynamics results are presented and discussed in section 3. Section 4 gathers the major conclusions.

2. Computational Details

We have utilized the QCT method as implemented in our own extensively adapted version of the VENUS96[37] codes. Calculations have been done for diatom−triatom translational energies over the range $1.0 \leq E_{tr}/\text{kcal mol}^{-1} \leq 20$, which are summarized in Table 1. They cover vibrational excitations ranging from the ground state energy to values close to the dissociation threshold in the case of O_3, and OH vibrational excitations for the most populated states in the atmosphere. In all cases, the initial rotational quantum number of the colliding OH has been fixed at the ground level ($j = 1$). Since the OH molecules are highly vibrationally excited, one expects to a first approximation the initial rotational excitation to play a minor role. In fact, such a behavior is likely to be similar to that reported elsewhere.[38,39] This does not imply that a study of the rotational excitation should not be interesting in itself as the use of initial state-selected conditions has recently been invoked as a potential explanation for the slight discrepancy between our previously reported QCT calculations[29] for the $OH + O_3$ reaction and thermalized ones[40] based on same potential energy surface but employing variational transition state theory. Thus, we omit heretofore the specification of the initial rotational state of OH, which will be set at $j = 1$. In turn, $E_v = \sum_{k=1}^{3} E_{v_k}$ denotes the total vibrational energy of O_3, with E_{v_k} indicating the energy content of the various vibrational normal modes of the triatomic molecule. Note that the chosen vibrational excitation energy range for $O_3(E_v)$ covers internal energies of the triatomic up to near dissociation, with the initial conditions having been defined through the standard fixed normal mode sampling procedure which is implemented as an option of VENUS96.[37] Note further that, as in previous works of this series, the rotational energy about each principal axis of inertia of O_3 has been taken as $k_B T/2$, while the rotational temperature has been assumed to be 300 K. This corresponds to an intermediate value in the range of temperatures $100 \leq T/K \leq 500$, which are likely to be the ones of major practical interest in atmospheric chemistry and combustion processes. The initial diatom−triatom separation has been fixed at $17a_0$ such as to make the interaction there essentially negligible, with working parameters for numerical integration and maximum value of the impact parameter (b_{max}) being determined according to the usual procedure. Batches of 2000 trajectories have then been carried out for each translational energy and initial vibrational combination, making a total of 144 000 trajectories.

The energetics of the involved processes are best seen from Figure 1, which indicates by the line segments on the reactants side the various vibrational combinations according to the HO_4 DMBE potential energy surface.[29] Note that the internal energy combination on the reactants side not only are quite above the energy of the transition state of reaction 1 but are higher than the energy of the product channels leading to $O_2 + O_2 + H$, and $O_2 + OH + O$ formation. This implies that the reactions 1−3 will be feasible over the complete range of translational energies.

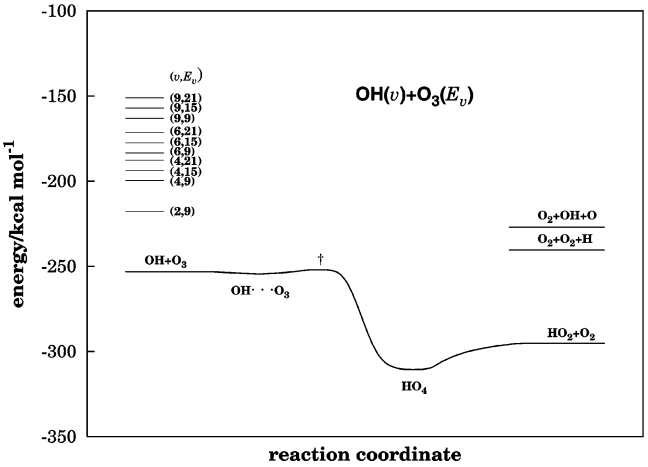

Figure 1. Schematic diagram showing the energetics of different processes according to the HO_4 DMBE potential energy surface.

For a given value of the translational energy, all relevant reactive cross sections and associated 68% uncertainties have been calculated. They will be denoted σ^x and $\Delta\sigma^x$, respectively, with x specifying the reaction outcome; $x = total$ stands for formation of $HO_2^*/HO_2 + O_2$, $O_2 + O_2 + H$, and $O_2 + OH + O$. From the cross sections, and assuming a Maxwell−Boltzmann distribution over the translational energy, the specific thermal rate coefficients are obtained as

$$k^x_{n_1,n_2}(T) = g_e(T)\left(\frac{2}{k_B T}\right)^{3/2}\left(\frac{1}{\pi\mu}\right)^{1/2}\int_0^\infty E_{tr}\sigma^x \exp\left(-\frac{E_{tr}}{k_B T}\right)dE_{tr} \quad (4)$$

where $n_1 = (v, j)$ and $n_2 = (E_v, E_{rot})$ denote specific vibrational−rotational states of OH and O_3 (in the present case $j = 1$, while E_{rot} is the rotational energy associated with a temperature of 300K), $g_e(T) = [1 + \exp(-205/T)]^{-1}$ is the electronic degeneracy factor that corresponds to the ratio of the electronic partition functions, k_B is the Boltzmann constant, and μ is the reduced mass of the colliding particles.

3. Results and Discussion

Table 1 provides a summary of the trajectory calculations reported in the present work. Column one indicates the vibrational combination, while the studied translational energies are in column two. For these initial translational energies, the dominant open reactive channels leading to products are

$$O_dH + O_aO_bO_c \rightarrow HO_dO_a + O_bO_c \quad (5)$$

$$\rightarrow HO_dO_c + O_aO_b \quad (6)$$

$$\rightarrow O_aO_b + O_cO_d + H \quad (7)$$

$$\rightarrow O_aO_d + O_bO_c + H \quad (8)$$

$$\rightarrow O_aO_b + O_dH + O_c \quad (9)$$

$$\rightarrow O_bO_c + O_dH + O_a \quad (10)$$

where the indices a, b, c, and d label the four different oxygen atoms. Note that in the case of HO_2^*/HO_2 formation, the reactions 5 and 6 have identical probabilities of occurrence, with

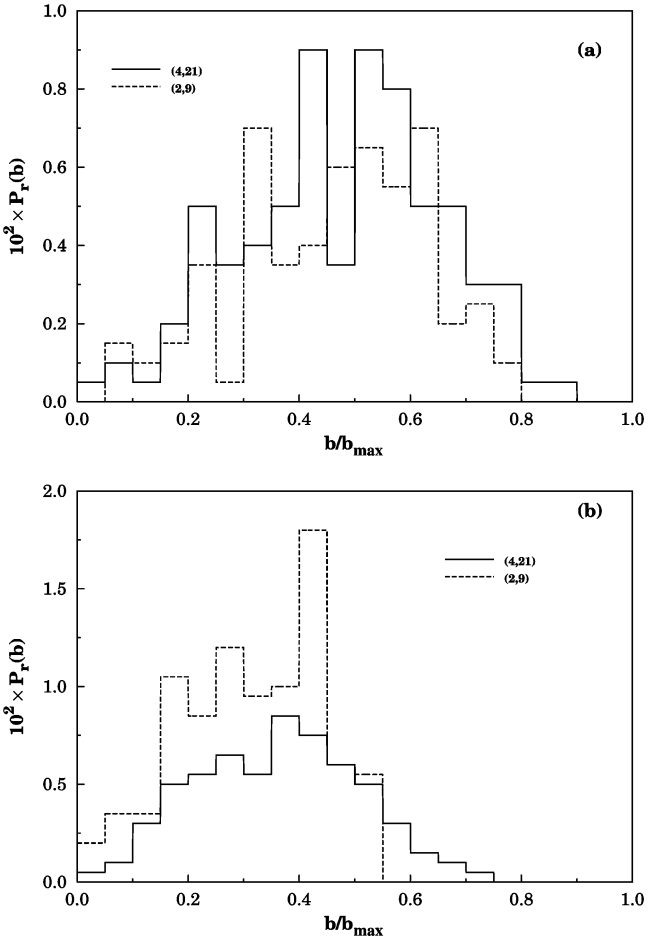

Figure 2. Opacity function for formation of HO_2^*/HO_2; (a) low collisional energy ("capture-type'') regime; (b) high collisional energy ("barrier-type'') regime.

any differences being attributable only to statistical errors in the QCT calculations. For the $O_2 + O_2 + H$, and $O_2 + OH + O$ formation, not only are the probabilities of reaction identical in eqs 7 and 8, but also are those of eqs 9 and 10. Note further that the probability of breaking the bonds increases in vibrationally excited O_3, and hence the formation of such products shows a significant growth. In summary, the processes leading to formation of $HO_2^*/HO_2 + O_2$,$O_2 + O_2 + H$, and $O_2 + OH + O$ hold a dominant position for the title multichannel reaction. For the higher vibrational energy combinations, formation of $O_2 + O_2 + H$ and $O_2 + OH + O$ may play a more prominent role than $HO_2^*/HO_2 + O_2$.

The dependences of the maximum impact parameter with translational energy is shown for the title reaction in Table 1. As expected, the maximum impact parameter increases with the internal energy of reactants for a fixed translational energy. Conversely, b_{max} is found to increase with decreasing translational energy, while, for higher translational energies, b_{max} is essentially constant, as it usually happens in reactions occurring via both capture-type and barrier-type mechanisms. These observations may be rationalized from the fact that the dominant interactions at low collision energies are of the long-range type. As for high translational energies, long-range forces are less important with increasing initial translational energy, hence leading only to small changes in b_{max}.

Figure 2 shows typical opacity functions for relatively low (a) and high (b) translational energies and vibrational combinations, namely (2, 9), and (4, 21). For clarity, only the cases

TABLE 2: Average Value of Scattering Angle in Degrees

(v, E_v)	E_{tr}/kcal mol^{-1}	$\langle\Theta_{scatt}\rangle$
(2, 9)	1.0	79.30
	2.0	82.82
	4.0	73.72
	6.0	72.76
	8.0	72.97
	12.0	81.98
(4, 9)	1.0	86.14
	2.0	84.39
	4.0	72.71
	6.0	74.60
	8.0	75.98
	12.0	76.06
(6, 9)	1.0	83.69
	2.0	77.08
	4.0	76.53
	6.0	70.79
	8.0	72.96
	12.0	82.11
(9, 9)	1.0	72.01
	2.0	86.50
	4.0	81.57
	6.0	74.40
	8.0	67.38
	12.0	77.28

corresponding to $E_{tr} = 1$ (panel a) and 12 kcal mol^{-1} (panel b) are shown. Note that the abcissae in these plots are b/b_{max}, with b_{max} being the largest impact parameter found in the present work ($11.72a_0$). One would expect two different patterns according to the translational energy regime: a bell shape for high translational energies as in the case of reactions that have a threshold energy (such a shape may be rationalized as due to the existence of a corresponding anti-threshold energy for formation of the products under analysis); a flat reaction probability with increasing impact parameter (up to the cutoff b_{max}) for reactions controlled by long-range forces. It turns out that substantial internal/translational energy mixing is expected on such collisional processes (especially when conducted using classical mechanics), which prevents a sharp distinction of such regimes and may explain the inefficiency of reaction for nearly head-on collisions (reorientation of the colliding species to follow the minimum energy path would then be unfavorable).

Table 2 contains the average values of the scattering angle[37] distribution in the reaction $OH + O_3 \rightarrow HO_2 + O_2$ for vibrational combinations (v, 9) at several translational energies. The significant observation is the small dependence of the average scattering angle on the translational/internal energy content of the reactants for the combinations here considered: 77.3° for (2, 9), 78.31° for (4, 9), 77.19° for (6, 9), and 76.52° for (9, 9).

The partitioning of energy release in the products of the reaction $OH + O_3 \rightarrow HO_2 + O_2$ has been carried out from the knowledge of the coordinates and velocities of each atom in the molecule in the center-of-mass frame of the molecule,[37] which are exhibited in Table 3. As shown, the outcoming HO_2 molecules have a considerable internal energy content, with a significant part of it being in the rotational degrees of freedom. Thus, part of vibrational energies in the reactants has been converted to rotational energy in the products. The notable feature is perhaps the fact that the average value of the vibrational energy of the HO_2 radicals represents more than half of the total energy of the products. Note that the average vibrational energy of the product HO_2^*/HO_2 species is much higher than the corresponding zero-point energy (ZPE). Thus, we may safely ignore in the present study the problem of ZPE

TABLE 3: Energies (in kcal mol^{-1}) Partitioned to Different Degrees of Freedom for Formation of $HO_2^*/HO_2 + O_2$

			HO_2^*/HO_2		O_2	
(v, E_{v_i})	E_{tr}	$\langle E_{tr}\rangle$	$\langle E_v\rangle$	$\langle E_r\rangle$	$\langle E_v\rangle$	$\langle E_r\rangle$
(2, 9)	1.0	13.81	49.41	9.18	3.97	1.92
	2.0	13.70	49.96	9.99	3.62	2.04
	4.0	15.76	50.61	9.66	3.26	2.01
	6.0	16.05	51.33	10.30	3.49	2.10
	8.0	17.21	51.84	11.51	2.63	2.08
	12.0	18.87	53.33	11.38	3.28	2.30
(4, 9)	1.0	20.82	55.06	13.44	3.81	3.21
	2.0	20.63	56.79	13.72	3.74	2.48
	4.0	22.15	56.81	13.66	3.73	3.03
	6.0	22.48	58.39	13.83	3.69	3.03
	8.0	24.47	57.72	15.25	2.85	3.06
	12.0	26.96	58.58	15.16	3.68	2.80
(6,9)	1.0	27.38	61.74	16.00	3.70	3.66
	2.0	25.90	63.65	16.88	3.57	3.56
	4.0	31.30	58.31	16.94	4.18	4.81
	6.0	25.91	65.31	18.48	3.91	3.96
	8.0	30.86	64.05	17.93	2.81	3.89
	12.0	31.53	65.74	18.70	3.45	3.98
(9,9)	1.0	31.31	76.37	17.25	3.98	4.06
	2.0	29.60	81.09	14.52	4.02	4.76
	4.0	34.11	73.86	17.49	4.24	6.22
	6.0	36.47	74.19	18.32	4.46	4.50
	8.0	36.10	81.78	14.02	3.96	4.15
	12.0	41.55	73.38	19.69	4.83	4.39

leakage (refs 8 and 36, and references therein). Also noteworthy is the percent of translational energy increase with increasing internal energy, representing up to one-third of the total energy of the products. It is then fair to conclude that most of the reactants initial internal energy is converted into vibrational and translational energy of the products.

We now examine the shapes of the calculated excitation functions (cross section vs translational energy) for the title reaction. These are shown in Figure 3 together with the associated 68% error bars. For simplicity, the O_3 vibrational energy content has been kept fixed at a given value, while the vibrational quantum number of OH(v) was allowed to vary over the whole range of values considered in the present work. As observed in previous studies of the title[36] and[8,41] OH(v') + $O_2(v'')$ reactions, two distinct trends are visible that may explain the observed shapes. At low translational energies, a capture-type regime dominates leading to the well-established decreasing dependence of σ^{total} on E_{tr}. At high energies, an increase of σ^{total} with E_{tr} is observed, which is typical of reactions with an energy threshold. As a result, the excitation function shows a minimum in the region where the two effects balance each other. Note that the energy ranges where the two distinct regimes dominate depend on the internal energies, as can be seen from the position where the minimum occurs.

To analytically describe the dependence of the cross section with the translational energy, we have adopted the form

$$\sigma^x(E_{tr}, E_{n_1}, E_{n_2}) = \frac{\sum_{i=1}^{3} c_i E_{sum}^{\ i}}{E_{tr}^{\ \alpha_1}} + \left(\sum_{j=0}^{3} d_j E_{sum}^{\ j}\right) E_{tr}^{\ \alpha_2} \exp(-\beta E_{tr}) \quad (11)$$

with

$$E_{sum} = E_{n_1} + E_{n_2} \quad (12)$$

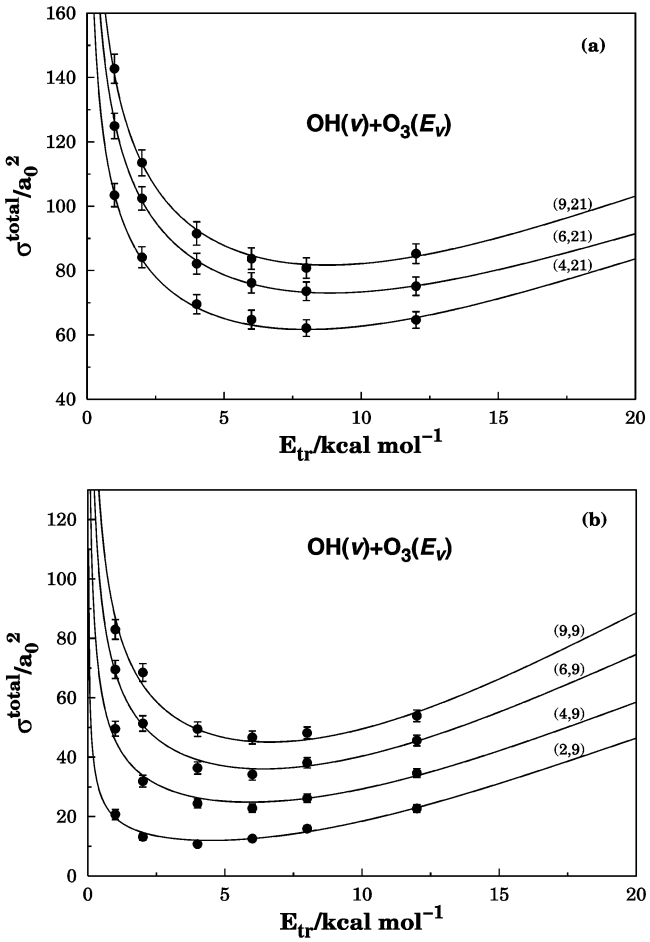

Figure 3. Specific cross section σ^{total} as a function of the translational energy. Also indicated are the 68% error bars and the fitted curves as given by eq 11: (a) (v, $E_v = 21$ kcal mol^{-1}); (b) (v, $E_v = 9$ kcal mol^{-1}).

TABLE 4: Numerical Values of Least-Squares Parameters in eq 11 (see also text)[a]

parameter	(v, 9)	(v, 21)
c_1	−0.49265	0.85145
c_2	3.83499(−2)	2.19326(−2)
c_3	−2.46039(−4)	−1.64068(−4)
d_0	0.10168	−0.12506
d_1	−3.24991(−3)	8.24004(−3)
d_2	6.19020(−5)	−1.14669(−4)
d_3	−3.16728(−7)	5.23532(−7)
α_1	0.44231	0.31790
α_2	2.57415	2.48279

[a] Units are the energy in kcal mol^{-1} and the cross section in a_0^2.

where E_{n_1} and E_{n_2} are the internal energies of OH and O_3 molecules. Note that such representation depends only on the internal energy of the reactant species but not on any specific model that expresses the dependence of the internal energy on quantum numbers. Except for $\beta = 0.05$, which has been optimized by trial and error, all the parameters have been determined from a least-squares fitting procedure, with their optimum values being reported in Table 4. The resulting fitted functions are exhibited together with the calculated points in Figure 3. It is seen that the fits show very good agreement with the points and hence reflect the general trends of the calculations. We emphasize that eq 11 is written in terms of E_{sum} and works equally well for all internal energy combinations here considered. Of course, it will only be accurate for the two fixed vibrational energies of ozone and hence cannot be used without risk to extrapolate to other values of this energy parameter.

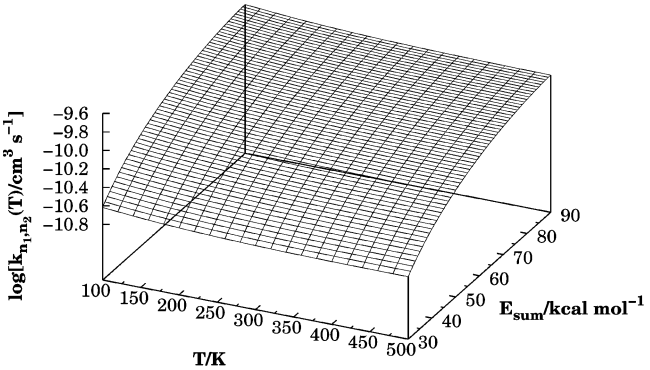

Figure 4. Total thermal rate coefficient for OH(v) + O_3(E_v = 9 kcal mol^{-1}) as a function of temperature and sum of the reactants internal energies.

TABLE 5: Calculated Thermally Averaged Total Rate Coefficients at Room Temperature, in cm^3 s^{-1}

(v, E_v)	E_{sum}/kcal mol^{-1}	k (T = 298 K)
(2, 9)	35.3	2.92(−11)
(4, 9)	53.4	6.78(−11)
(6, 9)	69.6	1.02(−10)
(9, 9)	90.0	1.29(−10)
(4, 15)	59.4	9.18(−11)
(6, 15)	75.6	1.27(−10)
(9, 15)	96.0	1.58(−10)
(4, 21)	65.4	1.47(−10)
(6, 21)	81.6	1.79(−10)
(9, 21)	102.0	1.99(−10)

By substitution of eq 11 in eq 4 and performing the integration analytically, one obtains for the specific thermal rate coefficients

$$k_{n_1,n_2}(T) = g_e(T)\left(\frac{8}{\pi\mu}\right)^{1/2} \times \left[(\sum_{i=1}^{3} c_i E_{sum}^{i})\Gamma(2-\alpha_1)(RT)^{-\alpha_1+1/2} + (\sum_{j=0}^{3} d_j E_{sum}^{\ j})\frac{\Gamma(\alpha_2+2)(RT)^{\alpha_2+1/2}}{(1+\beta RT)^{\alpha_2+2}}\right] \quad (13)$$

where Γ(...) is the gamma function, and all other symbols have their usual meaning. Figure 4 shows as a perspective plot of the OH(v) + O_3(E_v = 9) total reactive rate constant (i.e., for formation of products: HO_2^*/HO_2 + O_2, O_2 + O_2 + H, O_2 + OH + O), as a function of temperature and the sum of reactants internal energies. Note that similar considerations apply to the case of OH(v) + O_3(E_v = 21). Since their shapes differ only quantitatively, we show only the first case in Figure 4. For completeness, we provide in Table 5 the numerical values of the rate constant at 298 K for all combinations studied here. The notable feature from this table and Figure 4 is perhaps the significant increase of the rate constant with increasing reactant internal energy. However, such an increase is not monotonic with E_{sum}, as evidenced by the rates of the (6, 21) and (9, 15) combinations. At 298 K, they satisfy the relation k(6, 21) > k(9, 15), which is in reverse order with the corresponding values of E_{sum}. Thus, the way in which the internal energy is partitioned by the two colliding partners plays a role that cannot be modeled by the excitation function in eq 11, which depends only in E_{sum}. However, such a variation is likely to be reasonably small and hence has been ignored here for the sake of simplicity. We find though that, for a fixed vibrational energy of one of the reactant species, the rate constant increases with the vibrational excitation of its reactive partner. Finally, we address the implications of the minimum in the excitation function due to transition from a capture type regime to a barrier controlling one.[8,36,41] Such a minimum manifests in the present case also as a "dip" in the rate constant as a function of temperature for a fixed value of E_{sum}, after which the rate constant starts to increase (say, between 500 and 700 K for a fixed value of E_{sum} = 53.43 kcal mol^{-1}). Since this "dip" occurs for relatively high temperatures where the sampling of reactants initial conditions is perhaps questionable, it will not be shown in Figure 4; the reader is referred to ref 42 for a similar behavior in the case of the Cl^- + CH_3Br S_N2 reaction.

4. Conclusions

Despite its importance in environmental (atmospheric and combustion) chemistry, there is a paucity of knowledge concerning collisions of highly excited molecules, with important questions awaiting definitive answers. In particular, the title multichannel reaction has not been studied thus far, perhaps due to the lack, until recently, of a realistic potential energy surface for ground doublet HO_4. In this work, we have made the first attempt to bridge this gap by running trajectories for several combinations of vibrational excitation of the title system using the realistic DMBE potential energy surface from ref 29. The results suggest that the title multichannel reaction occurs both via capture- and barrier-type mechanisms, respectively, for low and high translational energies. They also predict the product HO_2^*/HO_2 radical to be formed with a substantial amount of internal energy (mostly of vibrational type) and the rate constants to be strongly influenced by the vibrational energy content of the reactant species. No comparison with experimental data has been possible (as such data are unavailable thus far), with the magnitude of the calculated rate constants suggesting that the title reaction may be of relevance in studying the stratospheric ozone budget as such high vibrationally excited species should be abundant at those altitudes.[12] Hopefully, the present work may stimulate measurements that employ laser techniques to prepare such vibrationally hot reactant species. Clearly, these experiments would be most welcome.

Acknowledgment. Financial support from Sichuan Provincial Science and Technology Fund for Distinguished Young Scholars and the Open Fund of State Key Laboratory of Oil and Gas Reservoir Geology and Exploitation (Southwest Petroleum University) is gratefully acknowledged. The financial support to one of us (A.J.C.V.) of Fundação para a Ciência e Tecnologia, Portugal, is also gratefully acknowledged.

References and Notes

(1) Muller, U.; Stock, G. *J. Chem. Phys.* **1997**, *107*, 6230.
(2) Weston, R. E.; Flynn, G. W. *Annu. Rev. Phys. Chem.* **1992**, *43*, 559.
(3) Gilbert, R. G.; Smith, S. C. *Theory of Unimolecular and Recombination Reactions*; Blackwell Scientific Publications: Oxford, 1990.
(4) Oref, I.; Tardy, D. C. *Chem. Rev.* **1990**, *90*, 1407.
(5) Gordon, R. *Comments At. Mol. Phys.* **1988**.
(6) Miller, R. L.; Suits, A. G.; Houston, P. L.; Toumi, R.; Mack, J. A.; Wodtke, A. M. *Science* **1994**, *265*, 1831.
(7) Rogaski, C. A.; Price, J. M.; Mack, J. A.; Wodtke, A. M. *Geophys. Res. Lett.* **1993**, *20*, 2885.
(8) Varandas, A. J. C. *Int. Rev. Phys. Chem.* **2000**, *19*, 199.
(9) Varandas, A. J. C. *Chem. Phys. Chem* **2002**, *3*, 433.
(10) Varandas, A. J. C. *J. Phys. Chem. A* **2004**, *108*, 758.
(11) Varandas, A. J. C. *J. Phys. Chem. A* **2005**, *109*, 2700.
(12) Varandas, A. J. C. *Chem. Phys. Chem* **2005**, *6*, 453.
(13) Wall, M. C.; Lemoff, A. S.; Mullin, A. S. *J. Phys. Chem. A* **1998**, *102*, 9101.
(14) Canty, T.; Pickett, H. M.; Salawitch, R. J.; Jucks, K. W.; Traub, W. A.; Waters, J. W. *Geophys. Res. Lett.* **2006**, *33*, L12802.
(15) Varandas, A. J. C. *Chem. Phys. Lett.* **2004**, *396*, 182.

(16) Finlayson-Pitts, B. J.; Kleindienst, T. E. *J. Chem. Phys.* **1981**, *74*, 5643.
(17) Greenblatt, G. D.; Wiesenfeld, J. R. *J. Geophys. Res.* **1982**, *87*, 11145.
(18) Shalashilin, D. V.; Umanskii, S. Y.; Gershenzon, Y. M. *Chem. Phys.* **1992**, *168*, 315.
(19) Rensberger, K. J.; Jeffries, J. B.; Crosley, D. R. *J. Chem. Phys.* **1989**, *90*, 2174.
(20) Raiche, G. A.; Jeffries, J. B.; Rensberger, K. J.; Crosley, D. R. *J. Chem. Phys.* **1990**, *92*, 7258.
(21) Sappey, A. D.; Copeland, R. A. *J. Chem. Phys.* **1990**, *93*, 5741.
(22) Dodd, J. A.; Lipson, S. J.; Blumberg, W. A. M. *J. Chem. Phys.* **1990**, *92*, 3387.
(23) Dodd, J. A.; Lipson, S. J.; Blumberg, W. A. M. *J. Chem. Phys.* **1991**, *95*, 5752.
(24) Chalamala, B. R.; Copeland, R. A. *J. Chem. Phys.* **1993**, *99*, 5807.
(25) Knutsen, K.; Dyer, M. J.; Copeland, R. A. *J. Chem. Phys.* **1996**, *104*, 5798.
(26) Zuhrt, C.; Zülicke, L. *Chem. Phys. Lett.* **1984**, *111*, 408.
(27) Caridade, P. J. S. B.; Zhang, L.; Garrido, J. D.; Varandas, A. J. C. *J. Phys. Chem. A* **2001**, *105*, 4395.
(28) Caridade, P. J. S. B.; Betancourt, M.; Garrido, J. D.; Varandas, A. J. C. *J. Phys. Chem. A* **2001**, 105, 7435.
(29) Varandas, A. J. C.; Zhang, L. *Chem. Phys. Lett.* **2000**, *331*, 474.
(30) Aoiz, F. J.; Bañares, L.; Herrero, V. J. *Int. Rev. Phys. Chem.* **2005**, *24*, 119.
(31) Varandas, A. J. C. in *Conical Intersections: Electronic Structure, Spectroscopy and Dynamics*, *Advanced Series in Physical Chemistry*; Domcke, W., Yarkony, D. R., H. Köppel, H., Eds.; World Scientific Publishing: Singapore, 2004; Chapter 5.
(32) Peiró-Garcia, J.; Nebot-Gil, J. *Comp. Phys. Comm.* **2003**, *4*, 843.
(33) Mansegas, A.; Anglada, J. M. *Comp. Phys. Comm.* **2006**, *7*, 1488.
(34) Engdahl, A.; Nelander, B. *J. Chem. Phys.* **2005**, *122*, 126101.
(35) Zhang, L.; Varandas, A. J. C. *Phys. Chem. Chem. Phys.* **2001**, *3*, 1439.
(36) Varandas, A. J. C.; Zhang, L. *Chem. Phys. Lett.* **2001**, *340*, 62.
(37) Hase, W. L.; Duchovic, R. J.; Hu, X.; Komornicki, A.; Lim, K. F.; Lu, D.; Peslherbe, G. H.; Swamy, K. N.; Linde, S. R. V.; Varandas, A. J. C.; Wang, H.; Wolf, R. J. *QCPE Bull.* **1996**, *16*, 43.
(38) Zhang, L.; Varandas, A. J. C. *J. Phys. Chem. A* **2001**, *105*, 10347.
(39) Zhang, L.; Varandas, A. J. C. *J. Phys. Chem. A* **2002**, *106*, 11911.
(40) Yu, L.; Han, K.; Varandas, A. J. C. *Int. J. Chem. Kinet.* **2006**, in press.
(41) Garrido, J. D.; Caridade, P. J. S. B.; Varandas, A. J. C. *J. Phys. Chem.* **1999**, *103*, 4815.
(42) Wang, Y.; Hase, W. L.; Wang, H. *J. Chem. Phys.* **2003**, *118*, 2688.